

Constraining SMEFT operators with associated $h\gamma$ production in Weak Boson Fusion

Anke Biekötter^{a,b}, Raquel Gomez-Ambrosio^{a,b}, Parisa Gregg^{a,b}, Frank Krauss^{a,b}, Marek Schönherr^a

^a*Institute for Particle Physics Phenomenology, Durham University, United Kingdom*

^b*Institute for Data Science, Durham University, United Kingdom*

Abstract

We consider the associated production of a Higgs boson and a photon in weak boson fusion in the Standard Model (SM) and the Standard Model Effective Theory (SMEFT), with the Higgs boson decaying to a pair of bottom quarks. Analysing events in a cut-based analysis and with multivariate techniques we determine the sensitivity of this process to the bottom-Yukawa coupling in the SM and to possible CP-violation mediated by dimension-6 operators in the SMEFT.

1. Introduction

The observation of the Higgs boson in 2012 [1, 2] initiated intense efforts to measure its properties in a wide range of production and decay processes, to either confirm it as the Higgs boson predicted by the Standard Model, or to catch first glimpses of new physics beyond it. To date, no significant deviation has been found [3, 4] and the Standard Model appears to be a robust and healthy theory. As a consequence the focus has shifted from the discovery of signals of new physics models to model-independent constraints on experimentally allowed deviations from Standard Model predictions.

In this work, we study the associated production of a Higgs boson with a photon in weak boson fusion (WBF), manifesting itself in a final state consisting of the two bosons and two forward jets. This process was first proposed as a possibly interesting Higgs boson production channel in [5, 6]¹. With the Higgs boson decaying into two b quarks, the additional photon efficiently suppresses otherwise dominant QCD backgrounds. The ATLAS collaboration has studied this channel in [7] with a boosted decision tree at 30.6 fb^{-1} and found a signal significance of 1.4σ . Using a cut-based analysis and contrasting it with multivariate techniques we analyse the potential of this channel for an independent measurement of the bottom-Yukawa coupling at higher luminosities.

We further investigate the impact of possible effects of beyond the Standard Model physics in WBF $h\gamma$ production, using the language of effective dimension-six operators from the Standard Model Effective Theory (SMEFT) [8–12]. Wilson coefficients of SMEFT operators relevant in Higgs physics have been constrained through various channels including WBF, for example in [13–38]. Here, we advocate to also use WBF production of the $h\gamma$ final state as an additional, independent constraint. While the kinematic structure of the interactions induced by CP-even

operators renders WBF Higgs boson production the by far preferred process, we focus in particular on CP-odd operators in the gauge-Higgs sector of SMEFT. They exhibit comparable sensitivity in both WBF h and $h\gamma$ production. In addition, the limits on this set of operators provides important constraints an additional sources of CP violation, necessary to describe, for example, electroweak baryogenesis [39–43]. The CP-odd dimension-6 EFT operators considered in our analysis have been studied and constrained in Higgs boson [44–48] and diboson production processes [49–52]. Our study further extends this list of relevant signatures and proposes a sensitive experimentally accessible observable, which we use to constrain two of the CP-odd operators of the dimension-6 EFT basis.

2. Signal and backgrounds in the Standard Model and determination of the b -Yukawa coupling

2.1. Process simulation

For our study we assume $\sqrt{s} = 13 \text{ TeV}$ throughout. The signal process ($h\gamma$ production in association with two jets at $\mathcal{O}(\alpha^4)$, both in the SM and in SMEFT) is simulated with `MadGraph5`, v2.6.6 [53] at leading order (LO) and with the default `NNPDF23_NLO` parton distribution function [54]. `PYTHIA 8.2` [55] models secondary emissions through parton showering, performs hadronization and adds the underlying event; it also decays the Higgs boson into the b -quarks. We select the WBF topology through the usual invariant mass cut on the tagging jets m_{jj} ; all jets, at both parton and hadron level, are defined through the anti- k_T algorithm [56] with $R = 0.4$. In the following, the indices j and b refer to the light and b -jets. At generation level the following parton-level cuts are applied to final-state transverse momenta p_T and pseudo-rapidities η

$$\begin{aligned} p_{T,j} &> 30 \text{ GeV}, & |\eta_j| &< 5., \\ p_{T,\gamma} &> 20 \text{ GeV}, & |\eta_\gamma| &< 2.5, \\ \Delta R_{\gamma j} &> 0.4, & m_{jj} &> 1200 \text{ GeV}. \end{aligned} \tag{1}$$

¹In this process, the hWW vertex is even more important than the hZZ coupling, compared to WBF h production.

The combination of these cuts ensures that non-WBF contributions (gluon fusion, $t\bar{t}h$ and Vh) to the signal are negligible at the 10% level [7].

All irreducible background processes are simulated at LO using *Sherpa*-2.2.7 [57] with the default NNPDF30_NNLO parton distribution function [58] from LHAPDF 6.2.1 [59]; matrix elements are calculated with COMIX [60] and jets are parton showered with CSSHOWER++ [61] [62]. For hadronisation etc. we use the *Sherpa* default settings.

Background contributions to the signal final-state feature the direct production of b -jets in the simulation, necessitating additional generation-level cuts. We consider the following processes:

- Continuum production of a b -jet pair, two light jets and a photon, $b\bar{b}jj\gamma$. In particular, we consider $\mathcal{O}(\alpha_s^4\alpha)$ contributions which we denote QCD and electroweak (EW) $Z\gamma jj$ production with the Z boson decaying to b -quarks, with the following additional cuts on the b 's:

$$\begin{aligned} p_{T,b} > 20 \text{ GeV}, \quad m_{bb} \in [90, 200] \text{ GeV}, \\ \Delta R_{\gamma b} > 0.4, \quad \Delta R_{jb} > 0.4, \end{aligned} \quad (2)$$

We have explicitly checked that the contributions from $\mathcal{O}(\alpha_s^2\alpha^3)$ are negligible at the 5% level and $\mathcal{O}(\alpha_s^3\alpha^2)$ as well as $\mathcal{O}(\alpha_s\alpha^4)$ contribute less than 1% each.

- $t\bar{t}\gamma$ production and single top production with an associated photon. For the $t\bar{t}\gamma$ and single top processes we force the decay of the W^\pm boson to light quarks. We do not apply specific cuts on the decay products of the on-shell top quarks, but we require, again,

$$\Delta R_{\gamma j} > 0.4 \quad (3)$$

for the single-top processes.

2.2. Extracting the signal

In the initial analysis with *Rivet* 2.7.0 [63] we apply the following baseline cuts to all signal and background processes:

1. We require an isolated photon with

$$p_{T,\gamma} > 20 \text{ GeV}, \quad |\eta_\gamma| < 2.5 \quad (4)$$

and the isolation given by

$$\sum_{i, \Delta R_{i\gamma} < 0.4} p_\perp^i < 10 \text{ GeV}. \quad (5)$$

2. We require exactly two light jets and two b -jets,

$$N_{\text{jets}} = N_{b\text{-jets}} = 2, \quad (6)$$

where both are defined with the anti-kT algorithm with $R=0.4$ and

$$\begin{aligned} p_{Tj} > 40 \text{ GeV}, \quad p_{Tb} > 30 \text{ GeV}, \\ |\eta_{j_1}| < 4.5, \quad |\eta_b| < 2.5. \end{aligned} \quad (7)$$

We assume perfect b -tagging efficiency.

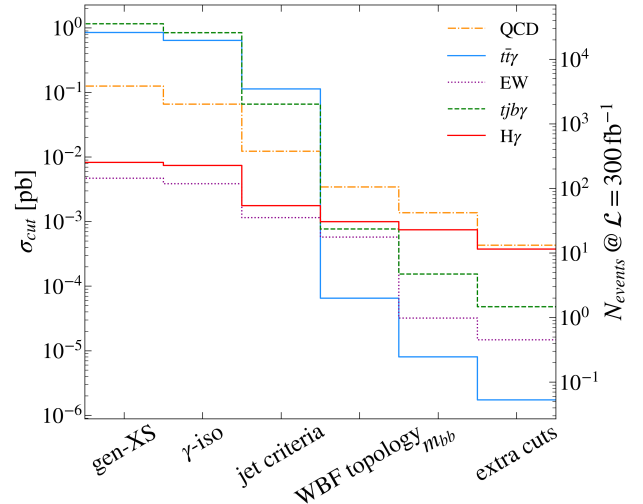


Figure 1: Cross section after different cuts in our cutflow, as given in Eqs. (4)-(10). On the right axis, we display the number of events for an integrated luminosity of 300 fb^{-1} . Be aware that we applied stronger cuts on the QCD and EW backgrounds at generator level which explains their lower generator-level cross section compared to the top backgrounds.

3. To select the WBF topology, we cut on the invariant light jet mass and the pseudo-rapidity difference of the light jets

$$m_{jj} > 1500 \text{ GeV}, \quad \Delta\eta_{jj} > 4.5. \quad (8)$$

4. We require the invariant b -jet mass to be close to the Higgs mass

$$m_{bb} \in [100, 140] \text{ GeV}. \quad (9)$$

This finalizes our baseline selection which we will use in the multivariate analysis in Section 2.3.

5. To allow for a fair comparison between a cut-and-count approach and the multivariate analysis below, we apply the following additional cuts in our cut-and-count analysis

$$\begin{aligned} |\eta_{j_1}| > 1.5, \quad |\eta_{j_2}| > 2, \\ \eta_{\gamma bb}^{\text{cen}}, \eta_\gamma^{\text{cen}}, \eta_{bb}^{\text{cen}} < 0.5, \\ m_{jj} > 2000 \text{ GeV}, \end{aligned} \quad (10)$$

where the centralities η_x^{cen} relative to the WBF tagging jets are defined as

$$\eta_x^{\text{cen}} = \left| \frac{\eta_x - \frac{\eta_{j_1} + \eta_{j_2}}{2}}{\eta_{j_1} - \eta_{j_2}} \right|. \quad (11)$$

The signal and background process cutflow is shown in Fig. 1. The baseline set of cuts, Eq. (9), reduces the contribution from $t\bar{t}\gamma$ and single top processes by six and four orders of magnitude, respectively, whilst only losing one order of magnitude in the signal. With the top-based backgrounds irrelevant after cuts, the dominant background

contribution for associated $h\gamma$ production stems from the continuum QCD process.

After the final cuts in Eq. (10), we reach a signal-over-background ratio of $S/B = 0.8$ in our cut-and-count analysis. We translate this into a CL_s limit [64] on the signal strength

$$\mu = \frac{\sigma(\text{pp} \rightarrow hjj\gamma) \text{BR}(h \rightarrow b\bar{b})}{\sigma^{\text{SM}}(\text{pp} \rightarrow hjj\gamma) \text{BR}^{\text{SM}}(h \rightarrow b\bar{b})} \quad (12)$$

using the CL_s limit setting implementation in **CheckMATE** [65]. The resulting limits are $\mu < 1.1$ for $\mathcal{L}_{\text{int}} = 30.6 \text{ fb}^{-1}$ at 95% CL ($\mu < 0.4$ for $\mathcal{L}_{\text{int}} = 300 \text{ fb}^{-1}$ and $\mu < 0.3$ for $\mathcal{L}_{\text{int}} = 3000 \text{ fb}^{-1}$) assuming negligible systematic uncertainties.

2.3. Determination of the b -Yukawa coupling

Since the coupling of the photon to quarks and gauge bosons as well as gauge-boson-quark couplings are very precisely known, the WBF $h\gamma$ signature will allow us to independently constrain the Higgs Yukawa coupling to the b -quark in the WBF topology.

To further increase the sensitivity to our search with respect to the final cuts in Eq. (10), we perform a multivariate analysis with **TMVA** [66] in **Root 6.22** [67]. We find the optimal signal regions – dependent on the luminosity – by passing the events satisfying the baseline selection cuts of Eq. (9) to a Boosted Decision Tree (BDT). Our pre-selection cuts are much stronger than the ones included in the experimental analysis in Ref. [7]. In particular, our cut on the invariant mass of the tagging jets $m_{jj} > 1500 \text{ GeV}$ is much tighter than the ATLAS constraint of $m_{jj} > 800 \text{ GeV}$, thereby effectively negating any effect of the $Z\gamma$ (EW) contribution. We generate $N = 200$ trees with a maximum depth of 3 and set the minimum node size to 6% to avoid over-training. As our input variables, we choose the p_T and η of all final-state particles, as well as

$$\begin{aligned} m_{jj}, \quad \Delta\eta_{jj}, \quad \Delta\phi_{jj}, \quad \Delta R_{\gamma,j_1}, \quad \Delta R_{\gamma,j_2}, \\ m_{bb}, \quad \Delta\eta_{bb}, \quad \Delta\phi_{bb}, \quad \Delta R_{\gamma,b_1}, \quad \Delta R_{\gamma,b_2}, \\ p_{T,bb}, \quad \eta_{bb}, \\ m_{bb\gamma}, \quad \Delta\eta_{\gamma,bb}, \quad \Delta\phi_{\gamma,bb}, \quad \Delta R_{\gamma,bb}, \\ \eta_{\gamma bb}^{\text{cen}}, \quad \eta_{\gamma}^{\text{cen}}, \quad \eta_{bb}^{\text{cen}}. \end{aligned} \quad (13)$$

As expected, the variable that is most often used by the BDT is m_{bb} which is peaked around the Higgs mass for the signal, but flat for the dominant QCD background. We have checked explicitly that after the cuts on the BDT classifier χ_{BDT} used for our limit setting we do not focus on a range of m_{bb} below the experimental detector resolution, cf. Fig. 2. All other input observables are less important individually, but collectively contribute much more than m_{bb} . Removing m_{bb} as an input variable altogether reduces the efficiency of the signal classification at a fixed background efficiency of 10% by about 10%. In Fig. 3 we

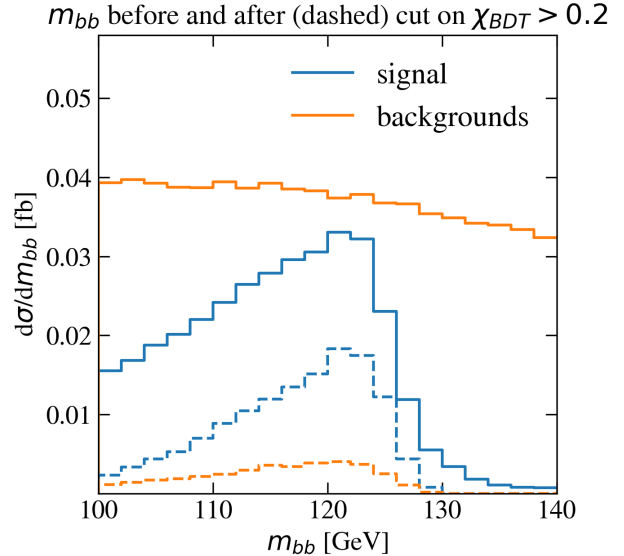


Figure 2: Distribution of the invariant mass of the b -jet pair m_{bb} before (solid lines) and after (dashed lines) a cut on the BDT classifier of $\chi_{\text{BDT}} > 0.2$.

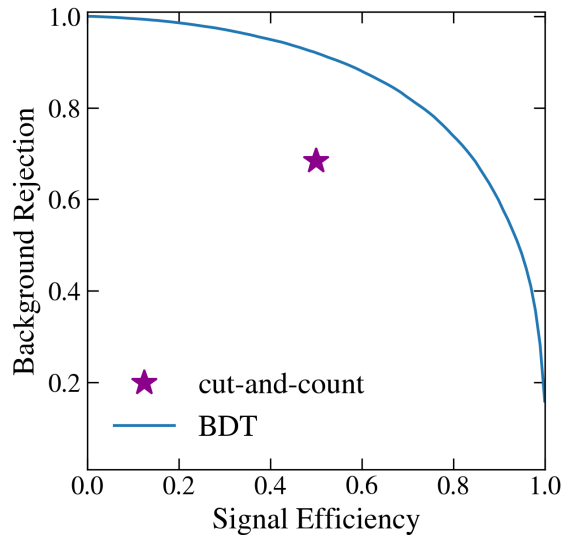


Figure 3: Receiver operating characteristic curve for the BDT analysis. The asterisk marks the signal and background efficiencies after the cuts in Eq. (10) compared to the baseline cuts, Eq. (9).

contrast the BDT ROC curve with the cut-and-count analysis efficiency. The BDT analysis clearly outperforms the cut-and-count approach for this rather complicated final state.

For a given luminosity, we choose the BDT classifier cut which minimizes the CL_s limit on the WBF $h\gamma$ signal strength μ . In our limit setting, we assume statistical uncertainties to be dominant and therefore neglect systematic uncertainties. For $\mathcal{L}_{\text{int}} = 30.6 \text{ fb}^{-1}$, the resulting 95% CL_s limit is $\mu < 0.8$ for a cut on the BDT classifier of $\chi_{\text{BDT}} > 0.1$. After this cut we are left with 6.2 expected signal and 2.8 expected background events. At $\mathcal{L}_{\text{int}} = 300 \text{ fb}^{-1}$ and $\mathcal{L}_{\text{int}} = 3000 \text{ fb}^{-1}$ these limits will in-

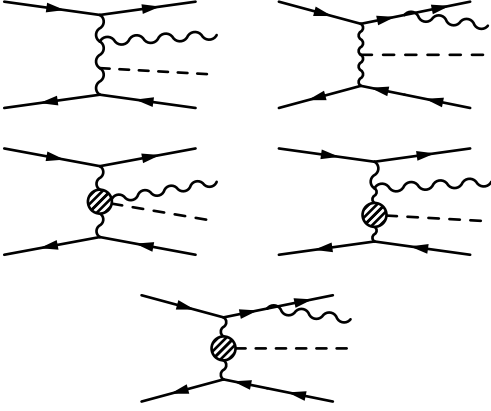


Figure 4: Example diagrams for WBF Higgs production in association with a photon in the SM (top row) and in the EFT (centre and bottom row).

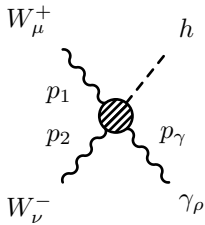
crease to $\mu < 0.25$ (for $\chi_{\text{BDT}} > 0.2$) and $\mu < 0.1$ (for $\chi_{\text{BDT}} > 0.2$), respectively. This clearly indicates that an observation of the decay channel $h \rightarrow b\bar{b}$ will be possible at the HL-LHC. Notice again, however, that the calculation assumes negligible systematic uncertainties which will no longer be true at higher luminosities. Assuming a 50% systematic uncertainty on the backgrounds, the above limits weaken to $\mu < 0.9, 0.3, 0.15$ at the 95% CL for integrated luminosities of $\mathcal{L}_{\text{int}} = 30.6 \text{ fb}^{-1}, 300 \text{ fb}^{-1}, 3000 \text{ fb}^{-1}$ respectively.

3. EFT analysis

3.1. Selection of operators

We continue with an analysis of potential BSM effects affecting the signal. Effects are, as usual, parametrized in terms of an effective Lagrangian, truncated at dimension-six [8–12, 68–70],

$$\mathcal{L}_{\text{SMEFT}} = \mathcal{L}_{\text{SM}} + \sum_i \frac{c_i \mathcal{O}_i^{(6)}}{\Lambda^2}, \quad (14)$$



$$\begin{aligned} c_{HWB} \frac{2iev s_\theta}{\Lambda^2} \frac{1}{c_\theta} (p_\gamma^\mu g_{\alpha\nu} - p_\gamma^\nu g_{\alpha\mu}) \\ c_{HW} \frac{-4iev}{\Lambda^2} (g_{\alpha\mu} (p_\gamma - p_1)^\nu + g_{\alpha\nu} (p_2 - p_\gamma)^\mu + g_{\mu\nu} (p_1 - p_2)^\alpha) \\ c_{HBW} \frac{-2iev s_\theta}{\Lambda^2} \frac{1}{c_\theta} \epsilon_{\alpha\nu\mu\rho} p_\gamma^\rho \\ c_{H\tilde{W}} \frac{4iev}{\Lambda^2} \epsilon_{\alpha\nu\mu\rho} (p_\gamma + p_1 + p_2)^\rho \end{aligned} \quad (16)$$

The Lorentz structure of the four-point interaction resulting from \mathcal{O}_{HW} is identical to the one from the SM $WW\gamma$ vertex. For this operator, the EFT and SM diagrams differ only by the additional t-channel W propagator in the

where the c_i are the Wilson coefficients. They correspond to the operators \mathcal{O}_i in the Warsaw basis [10] which are suppressed by inverse powers of the new physics scale Λ . Due to the relatively small cross section of our signal, many if not all of the Wilson coefficients of these operators will be constrained by other processes before our signal starts to become sensitive. In addition, in some other processes, trilinear boson couplings (such as VVV or VVh) experience high-momentum enhancement which is not the case for four-boson interactions, like $WW\gamma h$. However, our signal can provide an independent probe of paradigms underlying the construction of the effective field theory framework and may also help in lifting possible degeneracies in global fits.

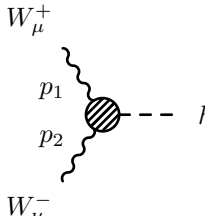
There are many operators contributing to our signal process, for example through their modifications of fermion-gauge or Higgs-gauge couplings. They can be tested (and better constrained) in WBF without an additional photon or other processes. Here, we will focus on operators which lead to contact interactions of three gauge bosons and a Higgs boson as depicted in the centre left diagram in Fig. 4, and the gauge-related subsets of effective three-point interactions. The diagrams with four-point interactions have the advantage of being suppressed by only two t-channel W propagators, compared to the SM which is suppressed by three t-channel W propagators when the photon is radiated from the W bosons and not from one of the quark lines. We can enhance their relative importance by requiring a large $\Delta R_{\gamma j}$ separation between the photon and the jets. A contact interaction of three gauge bosons and a Higgs boson exists for the following operators

$$\begin{aligned} \mathcal{O}_{HW} &= H^\dagger H W_{\mu\nu}^I W^{I\mu\nu} & \mathcal{O}_{H\tilde{W}} &= H^\dagger H \tilde{W}_{\mu\nu}^I W^{I\mu\nu} \\ \mathcal{O}_{HWB} &= H^\dagger \tau^I H W_{\mu\nu}^I B^{\mu\nu} & \mathcal{O}_{H\tilde{W}B} &= H^\dagger \tau^I H \tilde{W}_{\mu\nu}^I B^{\mu\nu}. \end{aligned} \quad (15)$$

The four-point interaction of three gauge bosons and a Higgs boson $WW\gamma h$ which results from these operators structurally looks like

SM case. The three-point VVh counterpart of the above operator has an additional momentum enhancement from derivatives in the $W_{\mu\nu}$ field strength tensors. For comparison, we show the structures of the WWh interaction

resulting from the operator \mathcal{O}_{HW} and its CP -odd counterpart $\mathcal{O}_{H\tilde{W}}$. The operators \mathcal{O}_{HWB} and $\mathcal{O}_{H\tilde{W}B}$ contribute to $hZ\gamma$, $h\gamma\gamma$ and hZZ couplings only. These couplings will be less relevant for our study because they do not allow for the photon to be radiated off the t -channel propagators and the contribution of diagrams in which the photon is radiated off a jet is suppressed by the cuts on the angle between the photon and the jets.



$$\begin{aligned}
c_{HW} & \frac{4iev}{\Lambda^2} (p_1^\nu p_2^\mu - g_{\mu\nu} p_1 \cdot p_2) \\
c_{H\tilde{W}} & \frac{4iev}{\Lambda^2} \epsilon_{\mu\nu\rho\delta} p_1^\rho p_2^\delta
\end{aligned} \quad (17)$$

Events for the EFT signal contributions have been generated with the SMEFTsim implementation [71] of the Warsaw basis with MadGraph [53], neglecting dimension-six squared terms. We apply the same cuts as for the SM signal. This includes the cuts in Eq. (1) on generator level, as well as the baseline selection cuts in Eq. (9) after parton showering and hadronization. After these cuts, we can parametrize the WBF $h\gamma$ cross section as

$$\begin{aligned}
& \frac{\sigma_{\text{SM}+1/\Lambda^2}^{(\text{LO})}}{\sigma_{\text{SM}}^{(\text{LO})}} \Big|_{\text{cuts}} - 1 \\
& = 10^{-3} \cdot \left(\frac{1 \text{ TeV}}{\Lambda} \right)^2 \cdot \left[-44 c_{HW} - 240 c_{HWB} \right].
\end{aligned} \quad (18)$$

The CP -odd operators do not contribute to the total cross section on the level of interferences of the EFT with the SM only. We will see in the next section how they can still have observable consequences for angular distributions of final state particles.

3.2. CP structure of the EFT and observable consequences

The vertex structures of the operators $\mathcal{O}_{H\tilde{W}}$ and $\mathcal{O}_{H\tilde{W}B}$, as given in Eq. (16), lead to CP violation. Currently, the best constraints on these operators in the Higgs sector come from observables in WBF and the Higgs decay $h \rightarrow ZZ \rightarrow 4\ell$ respectively [46]. For our process, we can construct CP -sensitive observables from combinations of scalar products and cross products of the momenta of the final state particles. As we have four particles in the final state, there are multiple ways to combine the momenta. Scanning over multiple combinations, we find the best sensitivity for a product of the momenta of the second p_T -ordered tagging jet, \vec{p}_{j_2} , the Higgs reconstructed from the two b -jets \vec{p}_{bb} and the photon \vec{p}_γ

$$\zeta = \frac{\vec{p}_\gamma \cdot (\vec{p}_{j_2} \times \vec{p}_{bb})}{|\vec{p}_\gamma| |\vec{p}_{j_2}| |\vec{p}_{bb}|}. \quad (19)$$

CP -odd operators create an asymmetry between the number of events with positive and negative ζ , which we denote

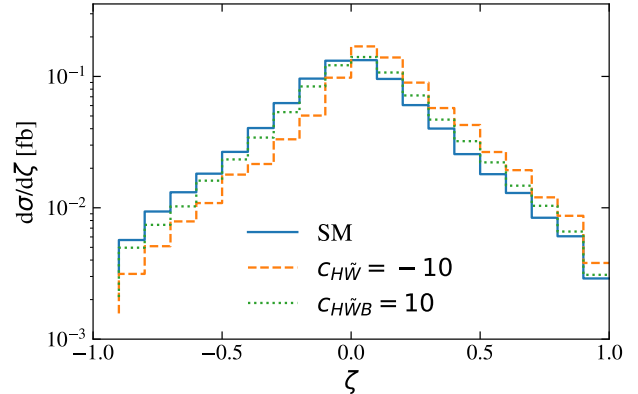


Figure 5: Distribution of the CP angle ζ in the SM and including the interference with the EFT.

by N_{ζ^+} and N_{ζ^-} respectively. In Fig. 5, we compare the distributions of ζ in the SM with the ones in the EFT for rather extreme values of the Wilson coefficients. While ζ is symmetric for the SM case, the EFT clearly introduces an asymmetry in it.

As discussed before, there is no contribution to the total cross section from the interference of the CP -odd EFT with the CP -even SM. Therefore, rather than studying the event numbers N_{ζ^\pm} directly, we examine their normalized asymmetries

$$A_\zeta = \frac{N_{\zeta^+} - N_{\zeta^-}}{N_{\zeta^+} + N_{\zeta^-}}, \quad A_\zeta^{\text{SM}} = 0. \quad (20)$$

After the baseline cuts of Eq. (9), we can parametrize the asymmetry in terms of the Wilson coefficients as

$$A_\zeta = 10^{-3} \cdot \left(\frac{1 \text{ TeV}}{\Lambda} \right)^2 \cdot \left[-39 c_{H\tilde{W}} + 12 c_{H\tilde{W}B} \right]. \quad (21)$$

Taking into account only the statistical uncertainty, this allows us to constrain the Wilson coefficients $c_{H\tilde{W}}$ and $c_{H\tilde{W}B}$ to

$$\frac{c_{H\tilde{W}}}{\Lambda^2} < \frac{1.1}{\text{TeV}^2} \quad \frac{c_{H\tilde{W}B}}{\Lambda^2} < \frac{3.6}{\text{TeV}^2} \quad \text{at 95\% CL.} \quad (22)$$

In principle, the magnitude of the asymmetry A_ζ depends on the kinematic region selected by our cuts, because the relative contributions of different diagrams can be enhanced in different regions. As an example, we display the dependence of the CP asymmetry on a cut on the invariant mass of the Higgs-photon pair $m_{bb\gamma}$ in Fig. 6. The asymmetry clearly rises with an increasing cut on $m_{bb\gamma}$.² However, as the cross section drops quickly with

²In our basis and assuming Lorentz gauge for the gauge bosons, the direct effective $WW h\gamma$ coupling fills the tails of the $m_{bb\gamma}$ distribution more efficiently than the dimension-six $WW h$ interaction, i.e. the $WW h\gamma$ coupling becomes more relevant at high $m_{bb\gamma}$.

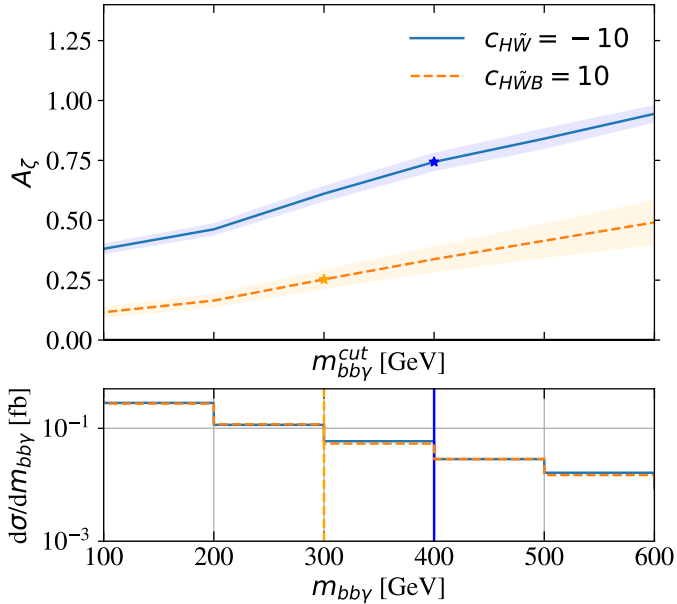


Figure 6: Dependence of the asymmetry A_ζ on a cut on the invariant mass of the Higgs-photon pair $m_{bb\gamma} > m_{bb\gamma}^{\text{cut}}$. The shaded band represents the statistical uncertainty on the asymmetry assuming an integrated luminosity of 3 ab^{-1} . The asterisk highlights the optimal cut on the invariant mass for the given Wilson coefficient. In the lower panel we show the distribution of the cross section as a function of the $m_{bb\gamma}$ invariant mass.

$m_{bb\gamma}$ as displayed in the lower panel of Fig. 6, the statistical uncertainty depicted by the shaded band around the asymmetry curve blows up rapidly. Therefore, the significance of the asymmetry measurement is a trade-off between selecting a signal region with a large asymmetry and keeping the measurement inclusive to reduce statistical uncertainties.

Assuming an optimal cut on the invariant mass of the Higgs-photon pair $m_{bb\gamma}$ (inclusive for $c_{H\tilde{W}}$ and $m_{bb\gamma} > 300 \text{ GeV}$ for $c_{H\tilde{W}B}$) we can improve the limits presented in Eq. (22) to

$$\frac{c_{H\tilde{W}}}{\Lambda^2} < \frac{1.1}{\text{TeV}^2} \quad \frac{c_{H\tilde{W}B}}{\Lambda^2} < \frac{3.1}{\text{TeV}^2} \quad \text{at 95\% CL.} \quad (23)$$

We can compare our results with the limits from a global fit of the Higgs sector including WBF without an extra photon [46], which for an integrated luminosity of 3 ab^{-1} are quoted as $|c_{H\tilde{W}}/\Lambda^2| < \frac{1.2}{\text{TeV}^2}$ and $|c_{H\tilde{W}B}/\Lambda^2| < \frac{1.5}{\text{TeV}^2}$.³ We would like to stress, though, our results for the limits are based on a comparison of SM $h\gamma$ production vs. the effect of SMEFT operators, and we did not include systematic uncertainties which we assume are larger for WBF+ γ than for WBF production alone.

³The quoted limits come from a global fit of the operators $\mathcal{O}_{H\tilde{W}}$, $\mathcal{O}_{H\tilde{W}B}$, $\mathcal{O}_{H\tilde{C}}$ and $\mathcal{O}_{H\tilde{B}}$. Since the limits on the Wilson coefficients of $\mathcal{O}_{H\tilde{C}}$ and $\mathcal{O}_{H\tilde{B}}$ stem mostly from gluon fusion Higgs production and the decay $h \rightarrow ZZ \rightarrow 4\ell$ the limits on $c_{H\tilde{W}}$ and $c_{H\tilde{W}B}$ in a one-parameter fit should not significantly differ from the ones of a global fit.

Although our simplified analysis of WBF $h\gamma$ does not clearly outperform the reference, the comparison underlines that a combination of our signal process with other signatures probing the same dimension-six operators is worth the effort, as it tests the underlying paradigms of the EFT construction and may lift degeneracies in a global fit.

4. Conclusions and Outlook

In this paper, we presented the prospects of measuring the b -Yukawa coupling or, conversely, the signal strength μ of the associated Higgs boson plus photon production in weak boson fusion with the Higgs boson decaying to bottom quarks at the LHC and the HL-LHC upgrade. The intricate kinematics of the five-particle final state render WBF $h\gamma$ production a prime candidate for the application of multivariate analysis techniques. In fact, the resulting limit on the signal strength is narrowed from $\mu < 1.1$ in a cut-and-count approach to $\mu < 0.8$ using a BDT analysis for the luminosity of the current ATLAS search $\mathcal{L}_{\text{int}} = 30.6 \text{ fb}^{-1}$. Tighter limits can be set with larger data sets, reaching $\mu < 0.25$ and $\mu < 0.1$ with $\mathcal{L}_{\text{int}} = 300 \text{ fb}^{-1}$ and $\mathcal{L}_{\text{int}} = 3000 \text{ fb}^{-1}$, respectively, neglecting systematic uncertainties. This clearly indicates the possibility of observing this process at higher luminosity.

We also investigate the potential of this signature to limit non-Standard-Model-couplings, parametrized in the SMEFT framework. Due to the presence of the additional photon compared to Higgs boson production in WBF only, the CP -even operators are four-boson operators and, thus, lack the additional momentum dependence of the three-boson vertices. Hence, we do not expect competitive limits on them.

The CP -odd operators, on the other hand, can be most meaningfully measured using asymmetries. Using A_ζ from Eq. 21 we extract the following limits

$$\frac{c_{H\tilde{W}}}{\Lambda^2} < \frac{1.1}{\text{TeV}^2} \quad \frac{c_{H\tilde{W}B}}{\Lambda^2} < \frac{3.1}{\text{TeV}^2} \quad (24)$$

at 95% CL with the full HL-LHC dataset of 3 ab^{-1} . Again, as the measurement of this signature will be statistically limited we have ignored systematic uncertainties.

Acknowledgements

We thank Filitsa Kougioumtzoglou for collaborating in the early stages of these studies. Our work is supported by the UK Science and Technology Facilities Council (STFC) under grant ST/P001246/1. FK and MS are acknowledging support from the European Union's Horizon 2020 research and innovation programme as part of the Marie Skłodowska-Curie Innovative Training Network MCnetITN3 (grant agreement no. 722104). MS is funded by the Royal Society through a University Research Fellowship, and FK gratefully acknowledges support by the

References

- [1] G. Aad, et al., Observation of a new particle in the search for the Standard Model Higgs boson with the ATLAS detector at the LHC, *Phys. Lett. B* 716 (2012) 1–29. arXiv:1207.7214, doi:10.1016/j.physletb.2012.08.020.
- [2] S. Chatrchyan, et al., Observation of a new boson at a mass of 125 GeV with the CMS experiment at the LHC, *Phys. Lett. B* 716 (2012) 30–61. arXiv:1207.7235, doi:10.1016/j.physletb.2012.08.021.
- [3] G. Aad, et al., Combined measurements of Higgs boson production and decay using up to 80 fb⁻¹ of proton-proton collision data at $\sqrt{s} = 13$ TeV collected with the ATLAS experiment, *Phys. Rev. D* 101 (1) (2020) 012002. arXiv:1909.02845, doi:10.1103/PhysRevD.101.012002.
- [4] A. M. Sirunyan, et al., Combined measurements of Higgs boson couplings in proton-proton collisions at $\sqrt{s} = 13$ TeV, *Eur. Phys. J. C* 79 (5) (2019) 421. arXiv:1809.10733, doi:10.1140/epjc/s10052-019-6909-y.
- [5] E. Gabrielli, F. Maltoni, B. Mele, M. Moretti, F. Piccinini, R. Pittau, Higgs Boson Production in Association with a Photon in Vector Boson Fusion at the LHC, *Nucl. Phys. B* 781 (2007) 64–84. arXiv:hep-ph/0702119, doi:10.1016/j.nuclphysb.2007.05.010.
- [6] D. M. Asner, M. Cunningham, S. Dejong, K. Randrianarivony, C. Santamarina, M. Schram, Prospects for Observing the Standard Model Higgs Boson Decaying into $b\bar{b}$ Final States Produced in Weak Boson Fusion with an Associated Photon at the LHC, *Phys. Rev. D* 82 (2010) 093002. arXiv:1004.0535, doi:10.1103/PhysRevD.82.093002.
- [7] M. Aaboud, et al., Search for Higgs bosons produced via vector-boson fusion and decaying into bottom quark pairs in $\sqrt{s} = 13$ TeV pp collisions with the ATLAS detector, *Phys. Rev. D* 98 (5) (2018) 052003. arXiv:1807.08639, doi:10.1103/PhysRevD.98.052003.
- [8] W. Buchmuller, D. Wyler, Effective Lagrangian Analysis of New Interactions and Flavor Conservation, *Nucl. Phys. B* 268 (1986) 621–653. doi:10.1016/0550-3213(86)90262-2.
- [9] H. Georgi, Effective field theory, *Ann. Rev. Nucl. Part. Sci.* 43 (1993) 209–252. doi:10.1146/annurev.ns.43.120193.001233.
- [10] B. Grzadkowski, M. Iskrzynski, M. Misiak, J. Rosiek, Dimension-Six Terms in the Standard Model Lagrangian, *JHEP* 10 (2010) 085. arXiv:1008.4884, doi:10.1007/JHEP10(2010)085.
- [11] R. Alonso, E. E. Jenkins, A. V. Manohar, M. Trott, Renormalization Group Evolution of the Standard Model Dimension Six Operators III: Gauge Coupling Dependence and Phenomenology, *JHEP* 04 (2014) 159. arXiv:1312.2014, doi:10.1007/JHEP04(2014)159.
- [12] I. Brivio, M. Trott, The Standard Model as an Effective Field Theory, *Phys. Rept.* 793 (2019) 1–98. arXiv:1706.08945, doi:10.1016/j.physrep.2018.11.002.
- [13] E. Massó, V. Sanz, Limits on anomalous couplings of the Higgs boson to electroweak gauge bosons from LEP and the LHC, *Phys. Rev. D* 87 (3) (2013) 033001. arXiv:1211.1320, doi:10.1103/PhysRevD.87.033001.
- [14] A. Falkowski, M. Gonzalez-Alonso, A. Greljo, D. Marzocca, Global constraints on anomalous triple gauge couplings in effective field theory approach, *Phys. Rev. Lett.* 116 (1) (2016) 011801. arXiv:1508.00581, doi:10.1103/PhysRevLett.116.011801.
- [15] G. Brooijmans, et al., Les Houches 2013: Physics at TeV Colliders: New Physics Working Group Report (2014). arXiv:1405.1617.
- [16] M. Trott, On the consistent use of Constructed Observables, *JHEP* 02 (2015) 046. arXiv:1409.7605, doi:10.1007/JHEP02(2015)046.
- [17] A. Falkowski, F. Riva, Model-independent precision constraints on dimension-6 operators, *JHEP* 02 (2015) 039. arXiv:1411.0669, doi:10.1007/JHEP02(2015)039.
- [18] G. Belanger, B. Dumont, U. Ellwanger, J. F. Gunion, S. Kraml, Global fit to Higgs signal strengths and couplings and implications for extended Higgs sectors, *Phys. Rev. D* 88 (2013) 075008. arXiv:1306.2941, doi:10.1103/PhysRevD.88.075008.
- [19] P. P. Giardino, K. Kannike, I. Masina, M. Raidal, A. Strumia, The universal Higgs fit, *JHEP* 05 (2014) 046. arXiv:1303.3570, doi:10.1007/JHEP05(2014)046.
- [20] S. Banerjee, S. Mukhopadhyay, B. Mukhopadhyaya, Higher dimensional operators and the LHC Higgs data: The role of modified kinematics, *Phys. Rev. D* 89 (5) (2014) 053010. arXiv:1308.4860, doi:10.1103/PhysRevD.89.053010.
- [21] B. Dumont, S. Fichet, G. von Gersdorff, A Bayesian view of the Higgs sector with higher dimensional operators, *JHEP* 07 (2013) 065. arXiv:1304.3369, doi:10.1007/JHEP07(2013)065.
- [22] P. Bechtle, S. Heinemeyer, O. Stål, T. Stefaniak, G. Weiglein, Probing the Standard Model with Higgs signal rates from the Tevatron, the LHC and a future ILC, *JHEP* 11 (2014) 039. arXiv:1403.1582, doi:10.1007/JHEP11(2014)039.
- [23] K. Cheung, J. S. Lee, P.-Y. Tseng, Higgs precision analysis updates 2014, *Phys. Rev. D* 90 (2014) 095009. arXiv:1407.8236, doi:10.1103/PhysRevD.90.095009.
- [24] J. Ellis, V. Sanz, T. You, Complete Higgs Sector Constraints on Dimension-6 Operators, *JHEP* 07 (2014) 036. arXiv:1404.3667, doi:10.1007/JHEP07(2014)036.
- [25] C. Englert, R. Kogler, H. Schulz, M. Spannowsky, Higgs coupling measurements at the LHC, *Eur. Phys. J. C* 76 (7) (2016) 393. arXiv:1511.05170, doi:10.1140/epjc/s10052-016-4227-1.
- [26] J.-B. Flament, Higgs Couplings and BSM Physics: Run I Legacy Constraints (2015). arXiv:1504.07919.
- [27] L. Bian, J. Shu, Y. Zhang, Prospects for Triple Gauge Coupling Measurements at Future Lepton Colliders and the 14 TeV LHC, *JHEP* 09 (2015) 206. arXiv:1507.02238, doi:10.1007/JHEP09(2015)206.
- [28] G. Buchalla, O. Cata, A. Celis, C. Krause, Fitting Higgs Data with Nonlinear Effective Theory, *Eur. Phys. J. C* 76 (5) (2016) 233. arXiv:1511.00988, doi:10.1140/epjc/s10052-016-4086-9.
- [29] S. Fichet, G. Moreau, Anatomy of the Higgs fits: a first guide to statistical treatments of the theoretical uncertainties, *Nucl. Phys. B* 905 (2016) 391–446. arXiv:1509.00472, doi:10.1016/j.nuclphysb.2016.02.019.
- [30] T. Corbett, O. J. P. Eboli, D. Gonçalves, J. Gonzalez-Fraile, T. Plehn, M. Rauch, The Higgs Legacy of the LHC Run I, *JHEP* 08 (2015) 156. arXiv:1505.05116, doi:10.1007/JHEP08(2015)156.
- [31] L. Reina, J. de Blas, M. Ciuchini, E. Franco, D. Ghosh, S. Mishima, M. Pierini, L. Silvestrini, Precision constraints on non-standard Higgs-boson couplings with HEPfit, *PoS EPS-HEP2015* (2015) 187. doi:10.22323/1.234.0187.
- [32] A. Butter, O. J. P. Éboli, J. Gonzalez-Fraile, M. C. Gonzalez-Garcia, T. Plehn, M. Rauch, The Gauge-Higgs Legacy of the LHC Run I, *JHEP* 07 (2016) 152. arXiv:1604.03105, doi:10.1007/JHEP07(2016)152.
- [33] J. de Blas, M. Ciuchini, E. Franco, S. Mishima, M. Pierini, L. Reina, L. Silvestrini, Electroweak precision observables and Higgs-boson signal strengths in the Standard Model and beyond: present and future, *JHEP* 12 (2016) 135. arXiv:1608.01509, doi:10.1007/JHEP12(2016)135.
- [34] J. de Blas, M. Ciuchini, E. Franco, S. Mishima, M. Pierini, L. Reina, L. Silvestrini, Electroweak precision constraints at present and future colliders, *PoS ICHEP2016* (2017) 690. arXiv:1611.05354, doi:10.22323/1.282.0690.
- [35] J. de Blas, M. Ciuchini, E. Franco, S. Mishima, M. Pierini, L. Reina, L. Silvestrini, The Global Electroweak and Higgs Fits in the LHC era, *PoS EPS-HEP2017* (2017) 467. arXiv:1710.05402, doi:10.22323/1.314.0467.
- [36] J. Ellis, C. W. Murphy, V. Sanz, T. You, Updated Global SMEFT Fit to Higgs, Diboson and Electroweak Data, *JHEP* 06 (2018) 146. arXiv:1803.03252, doi:10.1007/JHEP06(2018)146.

- [37] E. da Silva Almeida, A. Alves, N. Rosa Agostinho, O. J. P. Éboli, M. C. Gonzalez-Garcia, Electroweak Sector Under Scrutiny: A Combined Analysis of LHC and Electroweak Precision Data, *Phys. Rev. D* 99 (3) (2019) 033001. arXiv:1812.01009, doi:10.1103/PhysRevD.99.033001.
- [38] A. Biekötter, T. Corbett, T. Plehn, The Gauge-Higgs Legacy of the LHC Run II (2018). arXiv:1812.07587.
- [39] A. D. Sakharov, Violation of CP Invariance, C asymmetry, and baryon asymmetry of the universe, *Pisma Zh. Eksp. Teor. Fiz.* 5 (1967) 32–35, [*JETP Lett.* 5,24(1967)]; *Sov. Phys. Usp.* 34,no.5,392(1991); *Usp. Fiz. Nauk* 161,no.5,61(1991)]. doi:10.1070/PU1991v034n05ABEH002497.
- [40] V. A. Kuzmin, V. A. Rubakov, M. E. Shaposhnikov, On the Anomalous Electroweak Baryon Number Nonconservation in the Early Universe, *Phys. Lett.* 155B (1985) 36. doi:10.1016/0370-2693(85)91028-7.
- [41] M. E. Shaposhnikov, Baryon Asymmetry of the Universe in Standard Electroweak Theory, *Nucl. Phys.* B287 (1987) 757–775. doi:10.1016/0550-3213(87)90127-1.
- [42] A. E. Nelson, D. B. Kaplan, A. G. Cohen, Why there is something rather than nothing: Matter from weak interactions, *Nucl. Phys.* B373 (1992) 453–478. doi:10.1016/0550-3213(92)90440-M.
- [43] D. E. Morrissey, M. J. Ramsey-Musolf, Electroweak baryogenesis, *New J. Phys.* 14 (2012) 125003. arXiv:1206.2942, doi:10.1088/1367-2630/14/12/125003.
- [44] F. Ferreira, B. Fuks, V. Sanz, D. Sengupta, Probing CP-violating Higgs and gauge-boson couplings in the Standard Model effective field theory, *Eur. Phys. J. C* 77 (10) (2017) 675. arXiv:1612.01808, doi:10.1140/epjc/s10052-017-5226-6.
- [45] J. Brehmer, F. Kling, T. Plehn, T. M. P. Tait, Better Higgs-CP Tests Through Information Geometry, *Phys. Rev. D* 97 (9) (2018) 095017. arXiv:1712.02350, doi:10.1103/PhysRevD.97.095017.
- [46] F. U. Bernlochner, C. Englert, C. Hays, K. Lohwasser, H. Mildner, A. Pilkington, D. D. Price, M. Spannowsky, Angles on CP-violation in Higgs boson interactions, *Phys. Lett.* B790 (2019) 372–379. arXiv:1808.06577, doi:10.1016/j.physletb.2019.01.043.
- [47] C. Englert, P. Galler, A. Pilkington, M. Spannowsky, Approaching robust EFT limits for CP-violation in the Higgs sector, *Phys. Rev. D* 99 (9) (2019) 095007. arXiv:1901.05982, doi:10.1103/PhysRevD.99.095007.
- [48] V. Cirigliano, A. Crivellin, W. Dekens, J. de Vries, M. Hoferichter, E. Mereghetti, CP Violation in Higgs-Gauge Interactions: From Tabletop Experiments to the LHC, *Phys. Rev. Lett.* 123 (5) (2019) 051801. arXiv:1903.03625, doi:10.1103/PhysRevLett.123.051801.
- [49] J. Kumar, A. Rajaraman, J. D. Wells, Probing CP-violation at colliders through interference effects in diboson production and decay, *Phys. Rev. D* 78 (2008) 035014. arXiv:0801.2891, doi:10.1103/PhysRevD.78.035014.
- [50] S. Dawson, S. K. Gupta, G. Valencia, CP violating anomalous couplings in $W\gamma$ and $Z\gamma$ production at the LHC, *Phys. Rev. D* 88 (3) (2013) 035008. arXiv:1304.3514, doi:10.1103/PhysRevD.88.035008.
- [51] M. B. Gavela, J. Gonzalez-Fraile, M. C. Gonzalez-Garcia, L. Merlo, S. Rigolin, J. Yepes, CP violation with a dynamical Higgs, *JHEP* 10 (2014) 044. arXiv:1406.6367, doi:10.1007/JHEP10(2014)044.
- [52] A. Azatov, D. Barducci, E. Venturini, Precision diboson measurements at hadron colliders, *JHEP* 04 (2019) 075. arXiv:1901.04821, doi:10.1007/JHEP04(2019)075.
- [53] J. Alwall, R. Frederix, S. Frixione, V. Hirschi, F. Maltoni, O. Mattelaer, H. S. Shao, T. Stelzer, P. Torrielli, M. Zaro, The automated computation of tree-level and next-to-leading order differential cross sections, and their matching to parton shower simulations, *JHEP* 07 (2014) 079. arXiv:1405.0301, doi:10.1007/JHEP07(2014)079.
- [54] R. D. Ball, V. Bertone, S. Carrazza, L. Del Debbio, S. Forte, A. Guffanti, N. P. Hartland, J. Rojo, Parton distributions with QED corrections, *Nucl. Phys.* B877 (2013) 290–320. arXiv:1308.0598, doi:10.1016/j.nuclphysb.2013.10.010.
- [55] T. Sjöstrand, S. Ask, J. R. Christiansen, R. Corke, N. Desai, P. Ilten, S. Mrenna, S. Prestel, C. O. Rasmussen, P. Z. Skands, An Introduction to PYTHIA 8.2, *Comput. Phys. Commun.* 191 (2015) 159–177. arXiv:1410.3012, doi:10.1016/j.cpc.2015.01.024.
- [56] M. Cacciari, G. P. Salam, G. Soyez, The anti- k_t jet clustering algorithm, *JHEP* 04 (2008) 063. arXiv:0802.1189, doi:10.1088/1126-6708/2008/04/063.
- [57] T. Gleisberg, S. Hoeche, F. Krauss, M. Schonherr, S. Schumann, F. Siegert, J. Winter, Event generation with SHERPA 1.1, *JHEP* 02 (2009) 007. arXiv:0811.4622, doi:10.1088/1126-6708/2009/02/007.
- [58] R. D. Ball, et al., Parton distributions for the LHC Run II, *JHEP* 04 (2015) 040. arXiv:1410.8849, doi:10.1007/JHEP04(2015)040.
- [59] A. Buckley, J. Ferrando, S. Lloyd, K. Nordström, B. Page, M. Rüfenacht, M. Schönherr, G. Watt, LHAPDF6: parton density access in the LHC precision era, *Eur. Phys. J. C* 75 (2015) 132. arXiv:1412.7420, doi:10.1140/epjc/s10052-015-3318-8.
- [60] T. Gleisberg, S. Hoeche, Comix, a new matrix element generator, *JHEP* 12 (2008) 039. arXiv:0808.3674, doi:10.1088/1126-6708/2008/12/039.
- [61] S. Schumann, F. Krauss, A Parton shower algorithm based on Catani-Seymour dipole factorisation, *JHEP* 03 (2008) 038. arXiv:0709.1027, doi:10.1088/1126-6708/2008/03/038.
- [62] Z. Nagy, D. E. Soper, Matching parton showers to NLO computations, *JHEP* 10 (2005) 024. arXiv:hep-ph/0503053, doi:10.1088/1126-6708/2005/10/024.
- [63] A. Buckley, J. Butterworth, L. Lonnblad, D. Grellscheid, H. Hoeth, J. Monk, H. Schulz, F. Siegert, Rivet user manual, *Comput. Phys. Commun.* 184 (2013) 2803–2819. arXiv:1003.0694, doi:10.1016/j.cpc.2013.05.021.
- [64] A. L. Read, Presentation of search results: The CL(s) technique, *J. Phys. G* 28 (2002) 2693–2704, [11(2002)]. doi:10.1088/0954-3899/28/10/313.
- [65] D. Dercks, N. Desai, J. S. Kim, K. Rolbiecki, J. Tattersall, T. Weber, CheckMATE 2: From the model to the limit, *Comput. Phys. Commun.* 221 (2017) 383–418. arXiv:1611.09856, doi:10.1016/j.cpc.2017.08.021.
- [66] A. Hocker, et al., TMVA - Toolkit for Multivariate Data Analysis (2007). arXiv:physics/0703039.
- [67] R. Brun, F. Rademakers, ROOT: An object oriented data analysis framework, *Nucl. Instrum. Meth.* A389 (1997) 81–86. doi:10.1016/S0168-9002(97)00048-X.
- [68] S. Weinberg, Phenomenological Lagrangians, *Physica A* 96 (1-2) (1979) 327–340. doi:10.1016/0378-4371(79)90223-1.
- [69] H. Georgi, Weak Interactions and Modern Particle Theory, 1984.
- [70] J. F. Donoghue, E. Golowich, B. R. Holstein, Dynamics of the standard model, *Camb. Monogr. Part. Phys. Nucl. Phys. Cosmol.* 2 (1992) 1–540. doi:10.1017/CBO9780511524370.
- [71] I. Brivio, Y. Jiang, M. Trott, The SMEFTsim package, theory and tools, *JHEP* 12 (2017) 070. arXiv:1709.06492, doi:10.1007/JHEP12(2017)070.